Wake-field and fast head-tail instability caused by an electron cloud

K. Ohmi* and F. Zimmermann
CERN, Geneva, Switzerland

E. Perevedentsev
BINP, Novosibirsk, Russia

(Received 20 April 2001; revised manuscript received 12 July 2001; published 17 December 2001)

In positron and proton storage rings, electrons produced by photoemission, ionization, and secondary emission accumulate in the vacuum chamber during multibunch operation with close spacing. A positron or proton bunch passing through this ''electron cloud'' experiences a force similar to a short-range wake field. This effective wake field can cause a transverse-mode-coupling instability, if the electron-cloud density exceeds a threshold value. In this report, we compute the electron-cloud induced wake in a region without external magnetic field both analytically and via computer simulation, for parameters representing the low-energy positron ring of KEKB and the LHC proton beam in the CERN SPS. We study the linearity and time dependence of the wake function and its variation with the size of the electron cloud. Using a broadband resonator model for the electron-cloud wake field, we then evaluate theoretical expressions for the transverse-mode-coupling instability based on the linearized Vlasov equation, and for the instability threshold of fast transverse blow up including its dependence on chromaticity.

DOI: 10.1103/PhysRevE.65.016502 PACS number(s): 29.27.Bd, 29.20.Dh

I. INTRODUCTION

In positron and proton storage rings, an emittance growth has been observed in multibunch operation with close spacing ($\approx$10 ns) [1–3]. As a possible explanation, a single bunch instability caused by electron cloud has been discussed [4,5]. The instability has been analyzed using a formula of the fast electron-positron bunch instability [4,6], tracking simulation [5], and a simplified two-particle model [5]. In this paper, we study the wake force in more detail, evaluate the transverse-mode coupling caused by the electron cloud [7,8], and estimate instability thresholds for fast blow up.

Note that the electron-cloud effect we discuss is different from the electron-proton instability that has been observed at the Los Alamos PSR [9], where a fast transverse instability above a certain threshold current results in beam loss. The PSR stores a single proton bunch, with an rms length of about 25 m. Electrons inside the beam pipe perform many oscillations during the bunch passage, and their number can be strongly amplified at the trailing edge of the bunch (''trailing-edge multipactoring'' [10]). On the contrary, in this paper we consider a parameter regime that is characteristic of the LHC beam in the CERN SPS and of the two *B* factories, where short bunches, of mm or cm rms length, interact with a pre-established electron cloud, that has been generated by the preceding bunches. The number of electrons in the beam pipe does not change appreciably during the passage of a bunch, and electrons in the beam vicinity perform only about one oscillation along the bunch length. Thus, both the electron creation mechanism, the dynamics of the electron cloud, and the number of oscillations per bunch passage, which is a critical instability parameter, substantially differ from the Los Alamos case.

Further note that this instability is also different from both the ion-hose [11] and the fast beam-ion instability [6]. The ion-hose instability occurs if an electron beam is injected into a plasma, where the beam field expels the electrons. A two-stream instability can then develop between the generated plasma channel and the beam. The ion-hose instability is weakened by a solenoid field, which produces a cyclotron frequency comparable to the betatron frequency as determined by the plasma. By contrast, in this report we consider a positively charged beam passing through a non-neutral plasma of electrons. There is no guiding mechanism, and there are no ions. More and more electrons are attracted inside the beam volume during its passage. In addition, the betatron oscillation frequency is provided by external quadrupole fields and not by a plasma, and the effect of the electrons only constitutes a small perturbation, namely, it causes a shift in the fractional betatron tune. The difference to the fast beam ion instability is that, for the latter, the ions (or electrons) are generated during the passage of the bunch inside the beam volume, whereas in the electron-cloud case all electrons exist prior to bunch arrival and approximately uniformly fill the beam pipe prior to the bunch arrival.

We refer to a parameter regime where most of the electrons are formed by synchrotron radiation and photoemission or beam-induced multipacting. For LHC or KEKB, the number of electrons generated by ionization is about nine orders of magnitude lower. For this reason, the effect of ions on the cloud electrons is negligible [12].

The electron cloud induces a wake field when the beam passes through it; that is, a disturbance of the electron cloud, which is caused by a transverse perturbation of a longitudinal part of the beam, affects the following parts of the beam. In a storage ring, this wake field can induce two kinds of insta-

*On leave from KEK, Japan.

bilities. The medium range wake force ($>$ns) causes a transverse coupled-bunch instability [8], while the short-range wake ($<$100ps) causes a transverse single bunch instability, namely, a head-tail effect [5]. This paper addresses the short-range wake field.

We consider a bunch with distribution $\Psi(x,p_x,y,p_y,z,p_z;s)$ in the six-dimensional phase space, where the density Ψ is normalized so that $\int \Psi dx\, dp_x dy\, dp_y dz\, dp_z = 1$. The longitudinal coordinate z is the relative longitudinal displacement of beam. It is expressed by $z=s-ct$, where t is the arrival time of a particle with the longitudinal coordinate z at location s, and a positive z means the particle is ahead of the bunch center. A particle at a longitudinal position z in the bunch experiences a wake force from perturbations induced by the preceding part ($z' > z$) of the bunch. If the wake force $F_{x(y)}(z,s)$ is of the same nature as the wake arising from an ordinary impedance of vacuum chambers and cavities, it can be expressed by

$$F_{x(y)}(z,s) = \frac{N_+ r_c}{\gamma} \int_z^\infty W_{x(y)}(z-z',s)\rho_{x(y)}(z',s)\, dz' \quad (1)$$

where $\rho_{x(y)}(z,s) = \int dx\, dp_x dy\, dp_y dp_z x(y)\Psi$ is a horizontal (vertical) dipole moment at z, N_+ the number of positrons or protons in the bunch, r_c the classical particle radius, and γ the relativistic factor. The term $W_{x(y)}(z,s)$ is called the (dipole) wake field. This is the linear coefficient of the force coupled with a dipole moment of the preceding part of the bunch. In Eq. (1), a particle at longitudinal position z feels a force which depends only on the distance from the longitudinal position z' where a perturbation of the dipole moment occurs. The conventional instability formalism [13], as expressed by Eq. (1), relies on certain properties of the wake field, such as linearity, superposition, and time invariance. However, it is not clear *a priori* whether the wake field induced by the electron cloud has the same characteristics as the conventional one. A primary purpose in this paper is to study the characteristics of the wake force induced by the electron cloud and the accuracy at which it can be modeled by Eq. (1), i.e., treated like a normal wake field.

The electron cloud is formed by photoemission due to synchrotron radiation, due to residual-gas ionization by either the beam or the cloud itself, or due to secondary emission and beam-induced multipacting. The formation of the electron cloud has been studied previously in great detail, for positron and proton storage rings; see, e.g., Refs. [4,8,14,15]. Here we can use the information on the electron cloud obtained in the earlier studies. These have shown that for multibunch operation with close spacing ($\approx$10 ns) in positron rings the electron cloud buildup saturates near the neutralization level, at which, averaged over two or more bunch passages, there is no net force at the chamber wall. For certain values of bunch spacing and chamber aperture, similar densities also can be reached in proton rings, due to the secondary emission and multipacting. In the following study we consider a typical electron-cloud density of $\rho_c \approx 10^{12}$ m^{-3}, as we did in Ref. [5].

In this paper the wake force induced by the electron cloud is calculated for a region without external magnetic field, using both analytic and numerical methods. We employ the ''coasting beam'' approximation to evaluate the wake field; that is, the charge distribution of the beam is taken to be uniform in the longitudinal direction, where the line density of the positron bunch λ_b is given by $N_+/2\sigma_z$. In this approximation, the electrons oscillate in a constant beam potential near the beam center with an angular oscillation frequency of about

$$\omega_{e,x(y)} = \left(\frac{2\lambda_b r_e c^2}{\sigma_{x(y)}(\sigma_x+\sigma_y)} \right)^{1/2}, \quad (2)$$

where $\sigma_{x(y)}$ is the horizontal (vertical) beam size, r_e the classical electron radius, and c the speed of light. We attempt to model the wake field by a resonator, characterized by shunt impedance R_S, quality factor Q, and resonator angular frequency ω_R, as is commonly used for characterizing the impedance of vacuum chambers or cavities. We expect that, in the electron-cloud case, the resonant frequency of the equivalent resonator is closely related to the electron oscillation frequency ω_e.

Below the resonator parameters are evaluated, using either an analytical calculation or a simulation. The advantage of the simulation is that it includes some features which render the electron-cloud effect different from an ordinary wake field and which are neglected in the analytic treatment. These peculiar features are summarized as follows:

The strength of the wake force depends on the size of the electron cloud. Since the actual electron cloud is much larger than the beam, a more realistic estimate of the strength of the wake force can be obtained by the simulation.

The force between beam and electrons and, hence, also the effective wake force is nonlinear in the transverse perturbation amplitude. This nonlinearity will lead to a saturation of the instability at a certain amplitude, which is comparable to the beam size.

The electron cloud is distorted by the beam force as the interaction progresses. The effect of this distortion on the wake force can be estimated from the simulation.

We discuss the single bunch instability caused by the electron-cloud wake field by adapting the conventional instability theory, which is based on Eq. (1). This classical instability theory predicts an exponential growth whose rate is determined by the parameters of the beam and the wake field. Since the real wake field does not exactly fulfill Eq. (1), the actual instability has a behavior different from the simple exponential growth. We can conjecture the real behavior from the characteristics of the wake field obtained by the simulation. The tracking simulation reported in Ref. [5] included all of the above features correctly and explicitly. The approximations we make in this report are a trade off for the analytical approach.

Our discussion is done along the following steps. In Sec. II, the wake field is estimated by an analytic approach. The parameters R_S/Q and ω_R of the electron-cloud wake field are derived for the interaction between a rigid Gaussian bunch and a cloud with the same rms size. In this analytic estimate, the wake field has an infinite quality factor (Q). In other words, the excited electron cloud motion does not

TABLE I. Basic parameters of the KEKB LER and CERN SPS.

Variable	Symbol	KEKB-LER	SPS
Particle type	—	e^+	p
Circumference	L	3016 m	6900 m
Beam energy	E	3.5 GeV	26 GeV
Bunch population	N_b	3.3×10^{10}	7.5×10^{10}
Bunch spacing	t_{sep}	8 ns	—
rms beam sizes	σ_x	0.42 mm	5 mm
	σ_y	0.06 mm	3 mm
Bunch length	σ_z	5 mm	30 cm
rms energy spread	σ_E/E	0.0007	0.0011
Slippage factor	η	1.8×10^{-4}	5.78×10^{-4}
Chromaticity	$Q'_{x,y}$	4/8	—
Synchrotron tune	Q_s	0.015	0.006
Betatron tune	$Q_{\beta,x(y)}$	$\approx$46	26.7
Average beta function	$\beta_\perp$	15 m	40 m

damp in time. Next, in Sec. III, the wake force is calculated by a numerical approach. A simulation is performed following the same procedure as was used for studying the multibunch electron-cloud instability in Ref. [8]. The simulation allows the determination of R_S/Q and ω_R for an arbitrary cloud size. From this, we infer the relation of the wake-field parameters and the cloud size. In addition, nonlinear effects lead to a finite Q value, because the wake field damps over a few oscillation periods due to the electron frequency spread. The Q value is also obtained from the simulation. In Sec. IV, the transverse single bunch instability is studied using the approximate wake force determined in Sec. III. We analyze this instability using a perturbation formalism of the Vlasov equation, and estimate a threshold density of the electron cloud.

Wake force and instability growth rate are evaluated both for a positron ring and for a proton ring. To be specific, we use the parameters of the low-energy positron ring of the KEK B factory (KEKB-LER), and those of the CERN SPS operated with the LHC proton beam. In the positron ring, the bunches are flat and short ($2\sigma_z\approx1$ cm), while in the proton ring they are of nearly round shape and long ($\sigma_z>10$ cm). Relevant parameters of KEKB-LER and CERN-SPS are given in Table I. The oscillation frequencies of the electrons [Eq. (2)] multiplied by the bunch length, $\omega_e\sigma_z/c$, are 2.8 and 1.2 for vertical oscillation of KEKB-LER and CERN-SPS, respectively.

II. WAKE FORCE CALCULATED BY AN ANALYTIC APPROACH

We first discuss the wake force using an analytic approach. Slices of the positron beam are represented by their transverse center-of-mass coordinate at longitudinal coordinate z and location s as $[x_b(z,s),y_b(z,s)]$. Motion of the beam slice at z is described by the variation as a function of s. The electron cloud is characterized by its transverse center-of-mass $[x_c(s,t),y_c(s,t)]$ at location s. The motion of the electron cloud at s is described as a variation in time t.

In the analytical treatment, we assume that the beam-electron cloud interaction is linear in the displacement between the centers of beam and electron cloud at each s, where the beam slice at (z,s) interacts with the electron cloud at $[s,t=(s+z)/c]$. We here only consider the vertical motion. Extension to the horizontal motion is straightforward. The equations of motion for the beam and cloud are expressed as

$$\frac{d^2y_b(s,z)}{ds^2}+\left(\frac{\omega_{\beta,y}}{c}\right)^2 y_b(s,z) = -\left(\frac{\omega_{b,y}}{c}\right)^2\{y_b(s,z)-y_c[s,(s+z)/c]\}, \quad (3)$$

$$\frac{d^2y_c(s,t)}{dt^2}=-\omega_{c,y}^2[y_c(s,t)-y_b(s,ct-s)], \quad (4)$$

where $\omega_{\beta,y}$ denotes the angular betatron frequency without electron interaction. The two coefficients $\omega_{b,y}$ and $\omega_{e,y}$ characterize the linearized force between beam and cloud, and are given by

$$\omega_{b,y}^2=\frac{2\lambda_c r_e c^2}{\gamma k_y(\sigma_x+\sigma_y)\sigma_y}, \quad \omega_{c,y}^2=\frac{2\lambda_b r_e c^2}{k_y(\sigma_x+\sigma_y)\sigma_y}, \quad (5)$$

where λ_c and λ_b are the line densities of cloud and beam, and σ_x and σ_y are horizontal and vertical beam sizes, respectively. The coupling parameters ω_b and ω_c include a free parameter k_y, which is derived from the integration over two Gaussian distributions, representing beam and cloud. If the electron cloud is represented by a rigid Gaussian distribution with the same rms size as the beam, we have $k=2$. Note that ω_c, which is a coherent angular frequency of electron cloud, is different by the factor $1/\sqrt{k}\sim1/\sqrt{2}$ from the incoherent oscillation frequency of a single electron, ω_e in Eq. (2). The horizontal equations of motion are of the same form as the vertical ones, and are obtained by replacing $\omega_{b,y}$ and $\omega_{c,y}$ with

$$\omega_{b,x}^2=\frac{2\lambda_c r_e c^2}{\gamma k_x(\sigma_x+\sigma_y)\sigma_x}, \quad \omega_{c,x}^2=\frac{2\lambda_b r_e c^2}{k_x(\sigma_x+\sigma_y)\sigma_x}. \quad (6)$$

For the initial condition $y_c(s,-\infty)=0$, the solution of Eq. (4) is given as

$$y_c(s,t)=\omega_c\int_{-\infty}^{t} y_b(s,s-ct')\sin\omega_c(t-t')dt'. \quad (7)$$

Substituting the solution into Eq. (3), the equation for the beam motion is obtained as follows:

$$\frac{d^2y_b(s,z)}{ds^2}+\left(\frac{\tilde{\omega}_\beta}{c}\right)^2 y_b(s,z) = \frac{\omega_b^2\omega_c}{c^3}\int_z^\infty y_b(s,z')\sin\frac{\omega_c}{c}(z-z')dz'. \quad (8)$$

TABLE II. Analytically determined parameters for wake force induced by electron cloud using the resonator approximation. R/Q in units of Ω can be obtained by $cR_S/Q\times 30$. R_S/Q and ω_b^2, which linearly depend on ρ_c, are evaluated for $\rho_c=10^{12}$ m^{-3}.

	KEKB-LER		CERN-SPS	
	x	y	x	y
$\omega_c[\mathrm{s}^{-1}]$	6.4×10^{10}	1.70×10^{11}	8.9×10^{8}	1.15×10^{9}
$\omega_b[\mathrm{s}^{-1}]$	1.7×10^{5}	4.5×10^{5}	1.1×10^{5}	1.4×10^{5}
$cR_S/Q[\mathrm{m}^{-2}]$	1.5×10^{5}	2.9×10^{6}	3.9×10^{5}	8.3×10^{5}

Here $\tilde{\omega}_\beta^2=\omega_\beta^2+\omega_b^2$ is the angular betatron frequency including the interaction of the beam with the electron cloud. The corresponding coherent tune shift is expressed by

$$\Delta\omega_\beta=\frac{\omega_b^2}{2\omega_\beta}, \tag{9}$$

where ω_0 is the angular revolution frequency. The right-hand side of Eq. (8) can be represented by a wake function, which depends only on the longitudinal distance. Integrated over the ring circumference L, this wake function can be written

$$W_1(z)[\mathrm{m}^{-2}]=cR_S/Q\,\sin\left(\frac{\omega_c}{c}z\right) \quad \text{for} \quad z<0, \tag{10}$$

where

$$cR_S/Q=\frac{\gamma\omega_b^2\omega_c}{\lambda_b r_c c^3}L \tag{11}$$

and we have identified $\lambda_b y_b(s,z')=\rho_y(z',s)$ with ρ_y given in Eq. (1). Thus we have demonstrated that, under the approximations made, the wake field caused by the electron cloud can be represented by a resonator, as is generally used for impedance problems associated with cavities and vacuum chambers. If interpreted in terms of a resonator wake field, the coefficient of the sinusoidal wake function corresponds to a shunt impedance divided by a quality factor R_S/Q. In our linear model, the wake function does not damp. This means that, although R_S/Q is finite, both R_S and Q are infinite. For this analytical model, Eq. (8) also shows that the wake force obeys linearity and superposition principle for perturbation $y_b(s,z)$, and depends only on the longitudinal distance from the perturbation $(z-z')$.

Table II lists the parameters of the wake force computed for KEKB-LER and CERN-SPS. Here we have assumed that the electron-cloud line density of the analytical model, λ_c, is related to the electron density at the beam center by

$$\lambda_c=2\pi\sigma_x\sigma_y\rho_c. \tag{12}$$

This relation follows from an integration of a Gaussian distribution with rms size $\sigma_x\times\sigma_y$ and peak value ρ_c. The quantity R_S/Q in Table II linearly depends on ρ_c. In Table II, it has been evaluated for a density $\rho_c=10^{12}$ m^{-3}, which is a typical value found in simulations of the electron-cloud formation [4,5]. In addition, we have used $k_{x,y}=2$; this means that the beam and electron cloud were treated as rigid Gaussian distributions with equal transverse rms size. The actual size of the cloud is much larger than that of the beam. In this case, the parameter k should be larger than 2, and λ_c should also be larger. However, picturing the cloud as a rigid Gaussian with a much larger size than the beam is certainly not appropriate, due to the strong nonlinearity of the beam force at large amplitudes. Therefore, more realistic values of k and λ_c are determined by a numerical simulation described in the next section.

III. WAKE FIELD CALCULATED BY A SIMULATION

In this section, we estimate the wake force induced by the electron cloud using a computer simulation. The simulation takes into account some effects neglected in the analytic theory.

First, we study the relation of wake-field strength and cloud size. In the simulation, we include the electrons in the region of nonlinear force, i.e., at amplitudes $x>\sigma_x$ or $y>\sigma_y$. Note that a nonlinear interaction between the beam and each electron does not directly contradict with the assumed linearity of the collective interaction between beam and cloud. Electrons in the nonlinear region might simply contribute to the linear force between beam and cloud. In the previous section, the strength of the wake field R_S/Q was estimated from the line density of the cloud given in Eq. (12). The wake field was underestimated by omitting the contributions from electrons at larger amplitudes. The simulation on the other hand allows determining the strength of the wake field for an electron cloud widely distributed around the beam.

Second, we address the linearity of the wake force. The wake force is expected to be strongly nonlinear as a function of the perturbation amplitude, because of the nature of the beam-electron force. Specifically, the wake function should become weaker at large perturbation amplitudes, since the beam-electron force decreases for distances larger than the beam size. We study the linearity of the wake field by varying the amplitude of perturbation in the simulation, and from this we conjecture the saturation amplitude of the beam instability.

Third, the nonlinearity of the wake force also affects the quality factor Q of the wake field. The Q value was infinite for the analytical estimation. The nonlinearity of the interaction leads to a spread of resonant frequencies, with the result that Q is reduced to a finite value. In the simulation, the Q value can be estimated from the damping of the wake field obtained.

Fourth, we study the effect caused by the distortion of the cloud due to the beam. In the analytic estimation, the electron cloud was represented by its center-of-mass, and only the transverse dipole motion was considered. In reality, the beam force strongly distorts the electron-cloud distribution. Electrons are gathered near the beam center during the passage of the bunch [18]. The cloud density increases in a time interval of the order $1/\omega_e$. In the simulation, we study the variation of the wake field by changing the longitudinal po-

sition of a displaced bunch slice.

The electron density around 10^{12} m^{-3}, which we consider, is far smaller than the density of the beam, 10^{19} m^{-3} (KEKB) and 5×10^{15} m^{-3} (SPS). During the bunch passage the space-charge interaction between the electrons in the cloud, being much weaker than the beam-electron interaction, can, therefore, be neglected. Since the beam interacts with each electron independently, the wake force is proportional to the cloud density.

The simulation for the calculation of the wake force is performed following the same procedure as was used for studying the multibunch electron-cloud instability in Ref. [8]. We consider an electron cloud with a transverse size represented by macroparticles and a microbunch train with a very narrow spacing. Note that the microbunch train represents a ''coasting beam,'' i.e., a bunch with uniform longitudinal charge distribution. The macroelectrons are initialized with a transverse Gaussian distribution of a certain size, typically chosen as a multiple of the rms beam size. The motion of the macroparticles in the electron cloud is expressed by

$$\frac{d^2\boldsymbol{x}_{e,a}}{dt^2} = -\frac{2N_+ r_e c}{N_b}\sum_{i=1}^{N_p} \boldsymbol{F}_G(\boldsymbol{x}_{e,a}-\overline{\boldsymbol{x}}_{p,i};\boldsymbol{\sigma})\,\delta(t-t(s_b)), \tag{13}$$

where the force $\boldsymbol{F}_G(\boldsymbol{x})$ is expressed by the Bassetti-Erskine formula [16] normalized so that $\boldsymbol{F}_G\to\boldsymbol{x}/|\boldsymbol{x}|^2$ as $\boldsymbol{x}\to\infty$. N_b and $\boldsymbol{\sigma}$ are the number of particles in a microbunch and transverse beam size, respectively.

When microbunches pass through the center of cloud, they are not affected by the cloud and also the center-of-mass of the cloud does not move. If a microbunch with a small transverse displacement passes through the cloud, the cloud is perturbed and its center-of-mass changes. The subsequent microbunches are deflected by the perturbed cloud:

$$\overline{\boldsymbol{F}}(z_j,s) = \Delta\overline{\boldsymbol{x}'}_{p,j} = -\frac{2r_e}{\gamma}\sum_{a=1}^{N_e} \boldsymbol{F}_G(\overline{\boldsymbol{x}}(s)_{p,j}-\boldsymbol{x}_{e,a};\boldsymbol{\sigma}). \tag{14}$$

From Eq. (1), the wake force is calculated as the response to a small displacement of a microbunch, $[\rho_x(z),\rho_y(z)] = (x_{p,i},y_{p,i})\,\delta(z-z_i)$,

$$W_1(z_j,z_i) = \frac{\gamma}{N_b r_e}\frac{\Delta\overline{x'_{p,j}}}{\overline{x}_{p,i}} \quad \text{for} \quad z_j<z_i\,. \tag{15}$$

We compute the wake field for flat (KEKB-LER) and round (SPS) beams, and compare it with the analytical estimate. Microbunches are placed longitudinally every 0.1 mm and 1 mm for KEKB-LER and SPS, respectively. The actual bunches ($2\sigma_z=1$ cm and 60 cm) are represented by 100 and 600 microbunches for KEKB-LER and SPS, respectively. A microbunch corresponds to 3.3×10^8 and 1.25×10^8 real particles, respectively. In this simulation, the length of the beam (sequence of microbunches) is chosen to be longer than the actual bunch length. Needless to say, the charge line density is kept, and the total charge of the beam is thus larger than the actual bunch charge by a factor proportional to the bunch length. The electron cloud is modeled by macroparticles. We use 100 000 of macroparticles in the simulation, and we verified the robustness of the computation result by changing this number. The macroparticles are launched with a Gaussian distribution in the transverse plane, and their initial velocities are set to zero.

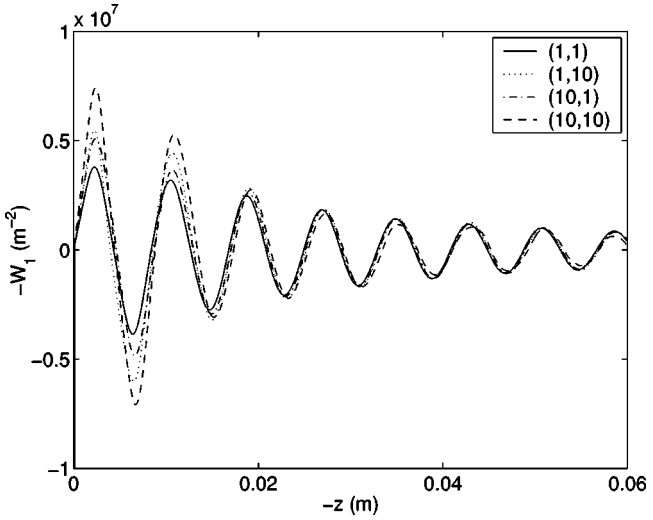

FIG. 1. Vertical wake force (W_1) induced by an electron cloud. Each line corresponds to a different size of the electron cloud: (1,1), (1,10), (10,1), and (10,10), in units of (σ_x,σ_y).

At first, the wake field is calculated by applying a displacement to the first microbunch ($i=1$), and we study how the wake field depends on the cloud size and on the perturbation amplitude. We later change the position of the displaced micro-bunch ($i>1$) and investigate the effect.

A. Wake field for flat beam

We investigate horizontal and vertical wake fields for a flat beam using the KEKB-LER parameters of Table I. The beam aspect ratio is $\sigma_x/\sigma_y=7$, a typical value for positron storage rings. As a consequence of the large aspect ratio, the horizontal and vertical wake fields have somewhat different characteristics.

We first study the dependence of the wake-field strength on the size of the electron cloud. The wake field is calculated for various sizes of the cloud maintaining a constant central density (ρ_c) and increasing the total number of cloud electrons (λ_c). The size of the electron cloud is characterized by two parameters (Σ_x,Σ_y) referring to the horizontal and vertical size in units of the rms beam size (σ_x,σ_y). For example, the line density λ_c for (a,b) is $a\times b$ times that of (1,1).

The vertical wake field is calculated by applying a vertical displacement of 0.05 mm to the first microbunch, Fig. 1 depicts the vertical wake force obtained by the simulation for various electron-cloud sizes: (1,1), (1,10), (10,1), and (10,10). The resonator parameters are determined by fitting the wake field to the expression [17]

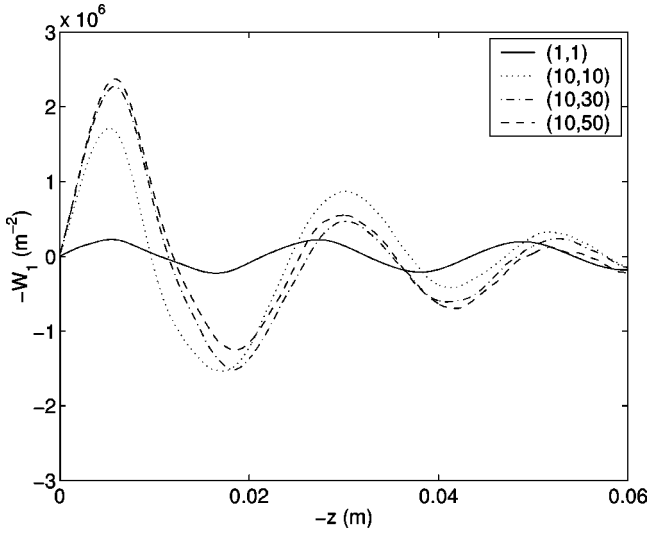

FIG. 2. Horizontal wake force (W_1) induced by an electron cloud. Each line corresponds to a different size of the electron cloud: (1,1), (10,10), (10,30), and (10,50), in units of (σ_x, σ_y).

$$W(z) = c\frac{R_S}{Q}\frac{\omega_R}{\bar{\omega}}\exp\left(\frac{\alpha}{c}z\right)\sin\left(\frac{\bar{\omega}}{c}z\right), \tag{16}$$

where $\alpha = \omega_R/2Q$ and $\bar{\omega} = \sqrt{\omega_R^2 - \alpha^2}$. Note that z is negative for the tail of the beam.

The wake field for (1,1) is described by $cR_S/Q = 4.0 \times 10^6\ \mathrm{m}^{-2}$, $\omega_R = 2.3\times 10^{11}\ \mathrm{s}^{-1}$, and $Q = 13$. These values are consistent with the analytic estimate [7], though cR_S/Q and ω_R are about 25% larger. The difference in frequency is reminiscent of the ''Yokoya factor'' known from the coherent beam-beam interaction [19].

The strength of the wake for (10,10) is two times larger than that of (1,1) over the first few oscillation periods. Note that the line density for (10,10) is 100 times larger than that of (1,1). The enhancement disappears after the third oscillation period, from which moment on all the lines coincide. The enhancement may be caused by electrons in the nonlinear region. It smears out rapidly, presumably due to filamentation of the nonlinear oscillations. We also calculated the wake forces for cloud sizes (1,5), (5,1), and (5,5). These showed good agreement with (1,10), (10,1), and (10,10), respectively, which suggests that electrons at amplitudes larger than 5σ do not contribute to the vertical wake.

We consider the wake field for (10,10) as the most accurate one, since the actual electron cloud is much larger than the beam. The parameters of the wake field are $cR_S/Q = 8.3\times 10^6\ \mathrm{m}^{-2}$, $\omega_R = 2.2\times 10^{11}\ \mathrm{s}^{-1}$, and $Q = 6.3$. The quality factor Q is finite in contrast to the analytic model. The reduction of Q is caused by the frequency spread of ω_R, or in other words, by the smear of the electron coherent motion, due to the nonlinearity of the beam-cloud interaction. The value of Q is smaller for larger cloud size. Electrons far from the beam experience a nonlinear force which approaches $1/r$ asymptotically. The contribution from these electrons will be smeared rapidly.

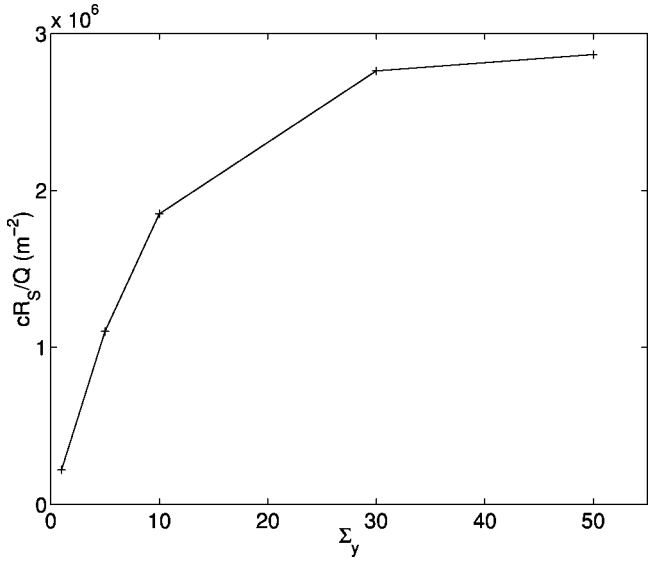

FIG. 3. Variation of cR_S/Q fitted from the simulation as a function of the vertical cloud size. The horizontal cloud size is held constant, equal to $10\times\sigma_x$.

The horizontal wake field is calculated in the same manner. We apply a horizontal displacement of 0.1 mm to the first microbunch. Figure 2 shows the wake field obtained by the simulation for various electron-cloud sizes. The wake force for (1,1) roughly coincides with the analytical estimate. We find $cR_S/Q = 2.2\times 10^5\ \mathrm{m}^{-2}$, $\omega_R = 8.7\times 10^{10}\ \mathrm{s}^{-1}$, and $Q = 60$. The horizontal wake field shows a rapid convergence when we increase the horizontal cloud size to 3 or $5\sigma_x$. On the other hand, the convergence with increasing vertical cloud size is poor, and the computed wake saturates only for vertical sizes as large as 30 to $50\sigma_y$.

This is demonstrated more clearly in Fig. 3, which shows the variation of the computed cR_S/Q as a function of the vertical cloud size. The value of the horizontal wake function for a large cloud size is much (13 times) higher than the analytic estimate of Sec. II.

We use the wake field obtained with a cloud size (10,50) as $cR_S/Q = 2.9\times 10^6\ \mathrm{m}^{-2}$, $\omega_R = 8.7\times 10^{10}\ \mathrm{s}^{-1}$, and $Q = 2.7$ for analyzing the instability. The quality factor is somewhat smaller than in the vertical plane. This may be due to the larger contribution from the nonlinear region.

In the analytical estimate based on the equal-size rigid Gaussian model, the wake force scales with the beam size as $cR_S/Q_{x(y)} \sim [(\sigma_x + \sigma_y)\sigma_{x(y)}]^{-3/2}$, which follows from Eqs. (5), (6), and (11). The horizontal wake force is much smaller, by a factor $(\sigma_y/\sigma_x)^{3/2} = 1/19$, than the vertical one. However, in the simulation the difference is only a factor of 2.9 for the wake force computed with the actual electron-cloud size of (10,10) in the vertical and (10,50) in the horizontal. This factor is close to $(\sigma_y/\sigma_x)^{1/2} = 1/2.65$. We may conjecture that the number of electrons, which contribute to the horizontal wake force, is not given by $\rho_c \times \sigma_x\sigma_y$, but by $\rho_c \times \sigma_x^2$. There is no large difference between the strength of the horizontal and vertical wake field. This means that not only the vertical instability, but also the horizontal one could be important. However, note that this conclusion will no longer hold, if

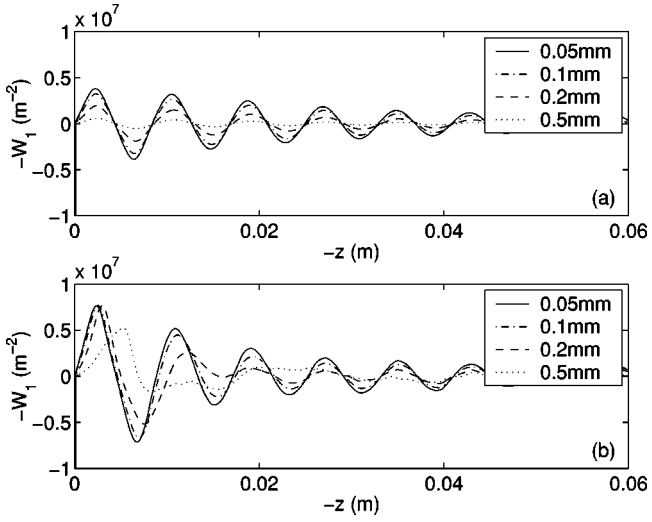

FIG. 4. Linearity of the vertical wake force induced by an electron cloud for a flat beam. Each line corresponds to a different displacement, of 0.05, 0.1, 0.2, and 0.5 mm. The vertical beam size is 0.06 mm. The two pictures refer to cloud sizes of (1,1) and (20,20), respectively.

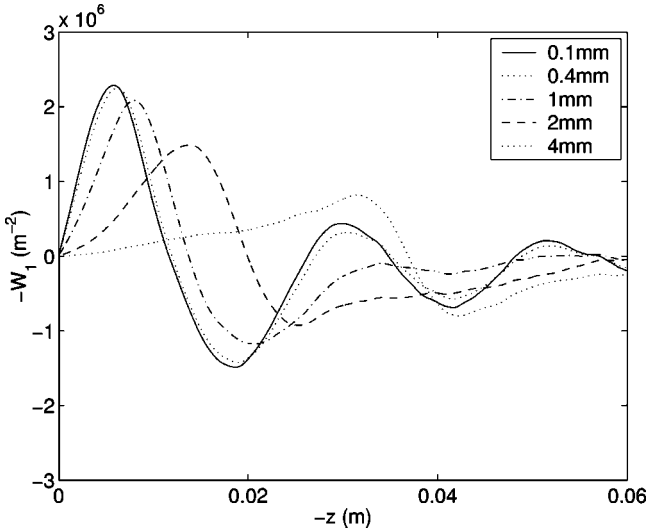

FIG. 5. Linearity of the horizontal wake force induced by an electron cloud for a flat beam. Each line corresponds to a different displacement, of 0.1, 0.4, 1, 2, and 4 mm. The horizontal beam size is 0.4 mm, and the electron-cloud size (20,50) in units of the two rms beam sizes.

there is a vertical magnetic field, since the latter suppresses the horizontal electron motion, but hardly affects the motion in the vertical plane.

We next discuss the linearity of the wake field in the perturbation amplitude. The wake field is expressed as the linear coefficient of the wake force F for a dipole perturbation $\rho_{x(y)}(z,s)$, as in Eq. (1). We calculate the wake force using Eqs. (13) and (15). However, the existence of a wake force does not guarantee the linearity of the perturbation. The linearity is examined by calculating the wake for various displacements of the first microbunch, as illustrated in Fig. 4. We study the linearity for two cloud sizes of (1,1) and (20,20). We choose (20,20) to avoid boundary effects for large amplitudes. In the figure, the wake forces are in agreement with each other at low amplitudes, while they deviate gradually at large amplitudes. The wake shows a good linearity at amplitudes below 0.1 mm for both cloud sizes. We conclude that the limit of the linearity is not related to the cloud size, but to the beam size. This means that instabilities will saturate at an amplitude comparable to the beam size.

Figure 5 shows the horizontal wake force computed for various initial displacements and a cloud size of (20,50). Also here the wake force displays a good linearity for small amplitudes, i.e., for amplitudes less than about 0.4 mm. We again infer that the limit of the linear range is determined by the beam size and independent of the cloud size.

The electron cloud becomes distorted due to the focusing force of the positron beam, on the time scale of $1/\omega_e$. In units of length, $c/\omega_{e,x}$ and $c/\omega_{e,y}$ correspond to 4.4 mm and 1.7 mm, respectively, for KEKB parameters.

We calculate the wake field for different longitudinal positions of the displaced micro-bunch. The sizes of electron cloud used are (10,10) and (10,50) for the vertical and horizontal wake force, respectively. Figure 6 shows the wake field for the displacement of a microbunch located a distance 0 mm, 2 mm, 4 mm, 6 mm, and 8 mm behind the head of bunch. Without focusing of the cloud by the beam, all lines should be identical. The difference between the lines reflects the distortion of the electron cloud due to the beam. For $-z \ll c/\omega_{e,y}=1.7$ mm, the wake force coincides with that for $-z=0$ mm. The disagreement is remarkable for increasing $-z$ (towards the tail of the bunch). The wake field can no longer be approximated by a resonator for large $-z$. It is sufficient to consider the behavior around <10 mm, because distances longer than the bunch length are of no interest. In Fig. 6, the amplitude of the vertical wake forces is enlarged 2.4 times at the maximum for the displacement of later microbunches. We attribute this enlargement to the focusing of the electron cloud, since $c/\omega_{e,y}<\sigma_z=4$ mm. On the other

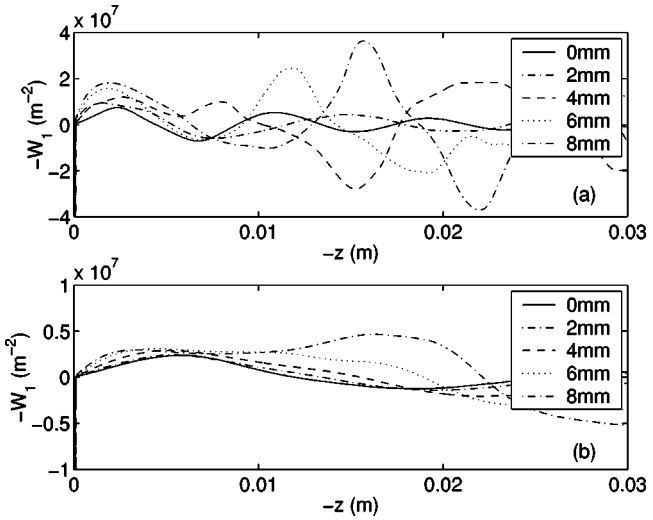

FIG. 6. Vertical and horizontal wake field computed by displacing microbunches at various longitudinal positions along the bunch, for electron-cloud sizes of (10,10) and (10,50), respectively.

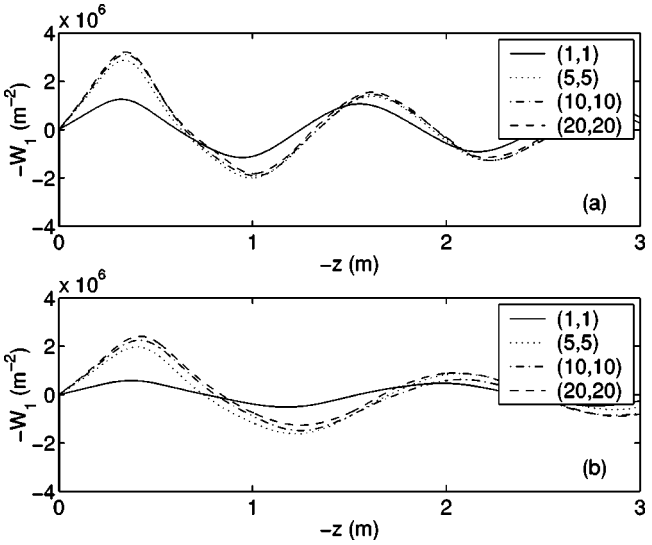

FIG. 7. Vertical and horizontal wake forces (W_1) induced by an electron cloud for an approximately round beam with an rms size of 5×3 mm^2. Each line corresponds to a different size of the electron cloud: (1,1), (5,5), (10,10), and (20,20), in units of the two rms beam sizes.

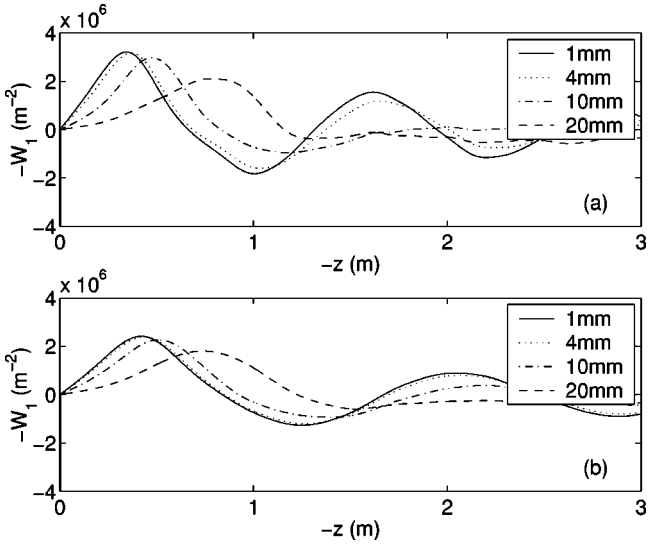

FIG. 8. Linearity of vertical and horizontal wake forces for an approximately round beam with a rms size of 5×3 mm^2 induced by an electron cloud. Each line corresponds to a different displacement of 1, 4, 10, 20, and 40 mm. The beam size is 5×3 mm^2, and the cloud size (10,10) in units of the two rms beam sizes.

hand, the horizontal field enlargement is smaller (5%) than the vertical one, presumably because $c/\omega_{e,x}\approx\sigma_z$.

B. Round beam

We now discuss the wake field caused by the electron cloud for a round beam. In proton rings, electron clouds formed by ionization and secondary emission may cause beam instabilities. In extremely high-energy proton rings such as LHC, synchrotron radiation and photoemission will also be important. The beam in a proton ring is often of nearly round shape. The characteristics of the round-beam wake force may be different from those of a flat beam. We calculate the wake field for the SPS parameters in Table I. The beam is approximately round (5×3 mm^2) with an aspect ratio of 0.6.

The wake field is calculated in the same manner as that of the flat beam. Figure 7 shows the vertical and horizontal wake field obtained by the simulation for various electron-cloud sizes. The wake-field parameters fitted in the case (1,1) are $cR_S/Q=1.3\times10^6$ m^{-2}, $\omega_R=1.5\times10^9$ s^{-1}, and $Q=16$ for the vertical plane, and $cR_S/Q=5.6\times10^5$ m^{-2}, $\omega_R=1.2\times10^9$ s^{-1}, and $Q=17$ for the horizontal. These numbers are roughly consistent with the analytic estimate. The computed wake force first grows for increasing cloud size, and then saturates for cloud sizes around 3–5σ. The parameters in the case (10,10) are $cR_S/Q=3.2\times10^6$ m^{-2}, $\omega_R=1.4\times10^9$ s^{-1}, and $Q=4.9$ for the vertical plane, and $cR_S/Q=2.6\times10^6$ m^{-2}, $\omega_R=1.1\times10^9$ s^{-1}, and $Q=3.5$ for the horizontal. The vertical and horizontal wake forces have similar characteristics. The maximum strength of the vertical wake force is 1.3 times that of the horizontal one, to be compared with an analytically estimated ratio of $(\sigma_x/\sigma_y)^{3/2}=2.1$. We should note here that the computed ratio of the wake strengths coincides with $(\sigma_x/\sigma_y)^{1/2}=1.3$, similar to the scaling found in the flat-beam simulation. In the next section, we use the wake field computed with a cloud size of (20,20) for the instability analysis.

Figure 8 shows the wake force computed with various initial displacements for cloud sizes of (20,20). They display a good linearity for amplitudes below 4 mm for either cloud size. Once again, we find that the range of the linear region is determined by the beam size and independent of the cloud size.

The length $c/\omega_{e,x}\approx c/\omega_{e,y}\approx20$ cm characterizes the time scale of cloud focusing. It is shorter than the bunch length $\sigma_z=30$ cm. We calculate the wake field varying the longitudinal position of the displaced microbunch in steps of 10

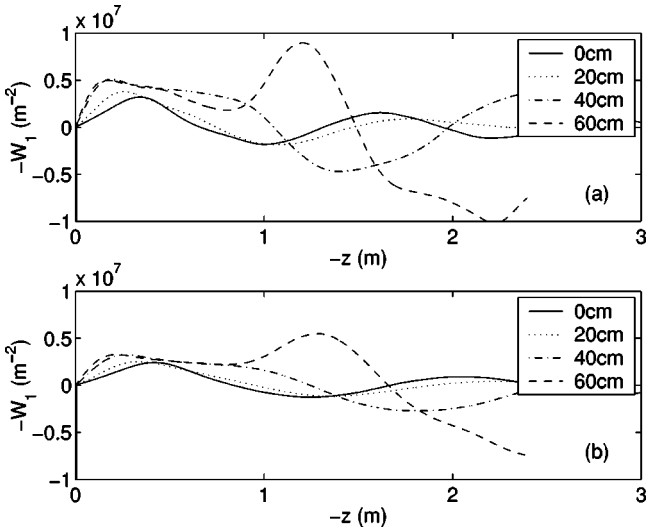

FIG. 9. Vertical and horizontal wake field computed for displacements of microbunches at various longitudinal positions, and an electron-cloud size of (20,20) in units of the two rms beam sizes.

TABLE III. Simulated parameters for the wake field induced by an electron cloud of density $\rho_e = 10^{12}$ m^{-3}, as obtained by fitting to the resonator model.

	KEKB-LER		SPS	
	x	y	x	y
ω_R[s^{-1}]	8.7×10^{10}	2.2×10^{11}	1.1×10^{9}	1.4×10^{9}
Q	2.7	6.3	3.5	4.9
cR_S/Q[m^{-2}]	2.9×10^{6}	8.3×10^{6}	2.6×10^{6}	3.2×10^{6}

cm. Figure 9 depicts the wake force computed for the displacement of a microbunch located a distance 0, 10, 20, 30, 40, 50, and 60 cm behind the head of the bunch. The figure shows that, if later microbunches are displaced, the wake field is enhanced by about 50%.

C. Summary for the wake field computed by the simulation

We calculated the wake field for flat-beam (KEKB-LER) and round-beam (CERN-SPS) using a simulation. From the simulation results depicted in Figs. 1, 2, and 7, we obtained the resonator parameters listed in Table III, which refer to the cloud sizes (10,50) and (10,10) for horizontal and vertical wake field of the flat beam, respectively, and (10,10) for the round beam. It is interesting to compare these numbers with the analytic estimates in Table II. The frequencies of the wake field are little changed from the analytical value. On the other hand, R_S/Q is increased by the contribution of electrons in the nonlinear region. Especially the horizontal wake of a flat beam is remarkably enlarged, by a factor of 13. The nonlinear force between beam and electrons, which causes a spread of ω_R, results in a finite Q factor. This Q was estimated by the simulation.

The transverse single bunch instability caused by the electron cloud can be analyzed using the wake fields of Table III. We stress that these wake fields are approximations:

(1) The wake field depends on the longitudinal position of the perturbation because of the focusing of the electron cloud due to the beam force, as discussed above. This longitudinal dependence introduces an ambiguity for the value of R_S/Q. From the simulation, the ambiguity is at most a factor of 2 for $c/\omega_R < \sigma_z$.

(2) We have used a coasting beam to calculate the wake field, but the actual beam particles are distributed as a Gaussian in the longitudinal phase space, and the real beam line density λ is not a constant.

(3) The transverse beam sizes $\sigma_{x(y)}$ vary as a function of s according to the local beta functions.

The variations of line density and beam size both cause a spread of ω_R, which will further reduce Q. Below we study the instability bearing in mind this uncertainty.

IV. TRANSVERSE SINGLE BUNCH INSTABILITY CAUSED BY THE WAKE FORCE

We now discuss a transverse single bunch instability caused by the wake force. This instability has been observed in simulation studies reported previously [5]. There, a clear instability threshold was observed, in either beam current or electron density, which was attributed to the onset of the strong head-tail or transverse-mode-coupling instability (TMCI). In order to confirm this hypothesis, we here analyze the instability using the perturbation theory of a Vlasov equation as is done for impedance problems due to vacuum chambers and cavities. A threshold density of electron cloud and growth of the instability can be estimated by the analysis. We use two methods to analyze the instability. One is the so-called TMCI theory [13], which is popularly used. In the theory, motion of a bunch is expanded into dipole betatron and its synchrotron side band modes,

$$\Psi = \sum_{l=-\infty}^{\infty} f(J_y, J_z) e^{i\phi_y} e^{il\phi_z} e^{-i\omega s/c}, \tag{17}$$

where J_i and ϕ_i are the action variables, amplitude and angle, of each phase space, respectively, and l is the azimuthal mode number of longitudinal motion, which characterizes a synchrotron side band. Stability of each mode is discussed by obtaining eigenvelues ω. The growth is caused by the mode coupling, and its rate is on the order of the synchrotron tune. The other is based on the coasting beam model in which the synchrotron motion is neglected [20,21]. The growth of the instability is explicitly assumed to be faster than the synchrotron period in this model. We call this approach the fast blow-up method. The threshold is determined by the relation between the growth of the instability and Landau damping. The tune spread due to the energy spread through the slippage and chromaticity contributes to the Landau damping. These two methods describe the same phenomenon, though their starting situations are different. The TMCI method has kept the time scale slower than the synchrotron period in mind, and brings up the threshold of instability whose growth time is on the order of the synchrotron period. The fast blow-up method starts to consider the time scale faster than the synchrotron period.

The instability has been studied by the tracking method in which beam-electron cloud interactions are calculated numerically for KEKB-LER [5,22,23]. The threshold of vertical instability was estimated to be $\rho_c \approx 5 \sim 10\times10^{11}$ m^{-3}. It is interesting to compare the threshold value.

We first analyze the instability using the TMCI approach. There are radial modes for J_z, which is characterized by Laguerre polynomials for Gaussian distribution on the longitudinal phase space. We take only the lowest radial mode and consider azimuthal mode coupling. The frequency (tune) of each mode $(\omega_{(l)} - \omega_\beta)/\omega_s$ is obtained by solving the eigenvalue problem for matrix M,

$$M_{ll'} = l\delta_{ll'} - i\frac{Nr_e c}{4\pi\gamma T_0 \omega_\beta \omega_s} i^{l-l'} \frac{1}{\sqrt{l!\,l'!}} \int_{-\infty}^{\infty} d\omega Z_1(\omega) \times \left[\frac{\omega\sigma_z}{\sqrt{2}c}\right]^{l+l'} \exp\left[-\frac{\omega^2\sigma_z^2}{c^2}\right]. \tag{18}$$

In Eq. (18), we use the impedance representation, which is the Fourier transform of the wake force,

$$Z_1(\omega)=i\int_{-\infty}^{\infty}\frac{dz}{c}e^{-i\omega z/c}W(z). \tag{19}$$

For given R_S, Q, and ω_R, the resonator impedance is expressed by

$$Z_1(\omega)=\frac{c}{\omega}\frac{R_S}{1+iQ\left(\frac{\omega_R}{\omega}-\frac{\omega}{\omega_R}\right)}. \tag{20}$$

The matrix in Eq. (18) has infinite dimension because of $l=-\infty,\infty$. The eigenfrequency $\omega_{(l)}\approx\omega_\beta\pm l\omega_s$ corresponds to a betatron side band. The real and imaginary parts of $\omega_{(l)}-\omega_\beta\mp l\omega_s$ denote tune shift and growth rate of each side band, respectively. When the real part becomes at a threshold $O(\omega_s)$, one mode couples or merges with another mode, and the two coupled modes assume imaginary frequency components and one of them becomes unstable. The imaginary part is also $O(\omega_s)$. This phenomenon is called the strong head-tail instability or mode-coupling instability [13].

We now truncate the matrix at $l=\pm 4$, and calculate the eigenvalues numerically. The eigenvalue or tune of each mode is computed as a function of R_S/Q using ω_R and Q of Table III. The strength of the wake field (R_S/Q) scales with the density of the electron cloud, since in our model each electron interacts with the beam independently. Figure 10 shows the computed mode-frequency variation as a function of R_S/Q. Since R_S/Q is linearly related with the cloud density ρ_c, the figure also gives us the dependence on ρ_c.

We observe that in each picture two frequencies corresponding to the betatron side bands ω_β and $\omega_\beta-\omega_s$ coincide at a certain value of cR_S/Q, i.e., the mode-coupling instability occurs. The threshold of the instability is characterized by $[cR_S/Q]_{x(y)}$ and corresponding electron cloud density $\rho_{\mathrm{thr},x(y)}$ for vertical and horizontal plane. They are expressed by

$$[cR_S/Q]_{\mathrm{thr},y}=2.7\times10^{7}\ \ \mathrm{m}^{-2}\quad \rho_{\mathrm{thr},y}\approx3.3\times10^{12}\ \ \mathrm{m}^{-3} \tag{21}$$

$$[cR_S/Q]_{\mathrm{thr},x}=4.8\times10^{6}\ \ \mathrm{m}^{-2}\quad \rho_{\mathrm{thr},x}\approx1.7\times10^{12}\ \ \mathrm{m}^{-3}. \tag{22}$$

The growth rate over ρ_{thr} behaves as $\sqrt{1-\rho/\rho_{\mathrm{thr}}}$. They are $\approx0.5\omega_s$ and $\approx0.03\omega_s$ for horizontal and vertical, respectively, at $\rho_c=2\rho_{\mathrm{thr}}$. We note that the vertical threshold $[cR_S/Q]_{\mathrm{thr}}$ is much higher than the horizontal one, and the vertical growth rate is much slower than the horizontal one. The matrix element of $M_{0,-1}$ is very small for $\omega_c\sigma_z/c>1$ and $Q\gg1$, as can be seen when integrating Eq. (18). It is difficult to compute mode coupling accurately for such a small coupling term. However, the description does not seem to be entirely correct in this case, and possibly we would need to take into account higher-order radial and azimuthal modes. We conjecture that the actual threshold of the vertical instability is lower than computed.

The coupled modes of $l=0$ and $l=-1$ separate again at $cR_S/Q=5\times10^{7}\ \mathrm{m}^{-2}$, as is seen in Fig. 10(a). However, from this we cannot conclude that the beam is stable again for these large values of cR_S/Q, since higher-order radial modes may also become important.

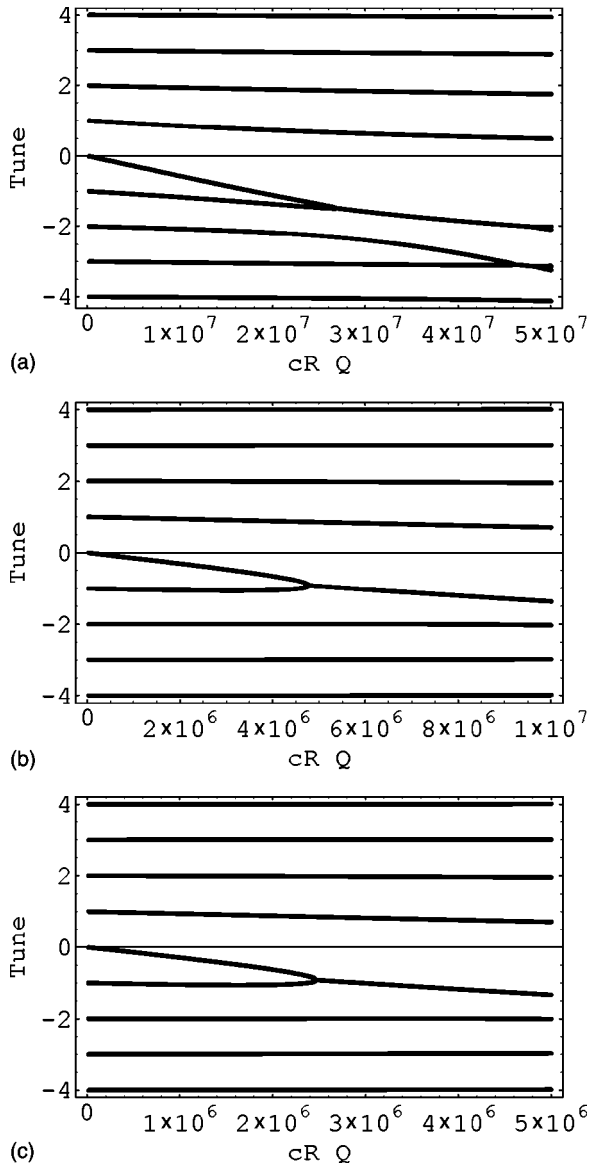

FIG. 10. Variation of the betatron side band frequencies $(\omega-\omega_\beta)/\omega_s$ with cR_S/Q, or cloud density, for constant values Q and ω_R taken from Table III. The chromaticity is zero. Pictures show (a) vertical and (b) horizontal side band spectra for the KEKB-LER, and (c) vertical spectra for the SPS.

In the case of the SPS, the computed threshold values are

$$[cR_S/Q]_{\mathrm{thr},y}=1.4\times10^{6}\ \ \mathrm{m}^{-2},\quad \rho_{\mathrm{thr},y}\approx4.4\times10^{11}\ \ \mathrm{m}^{-3}, \tag{23}$$

$$[cR_S/Q]_{\mathrm{thr},x}=1.0\times10^{6}\ \ \mathrm{m}^{-2},\quad \rho_{\mathrm{thr},x}\approx3.8\times10^{11}\ \ \mathrm{m}^{-3}. \tag{24}$$

The growth rates for both planes are $\approx0.5\omega_s$ at $\rho_c=2\rho_{\mathrm{thr}}$.

As discussed in Sec. III, the wake-field parameters R_S/Q and Q, listed in Table III, are somewhat uncertain. Considering the effect of the electron-cloud focusing due to the

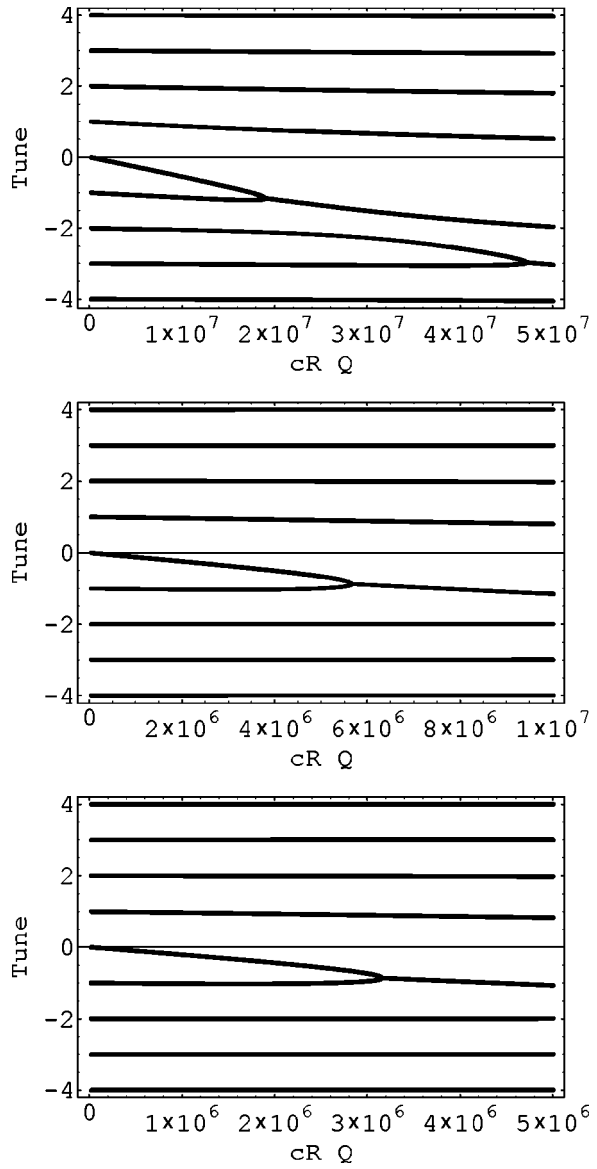

FIG. 11. Variation of the betatron side band frequencies $(\omega - \omega_\beta)/\omega_s$ with cR_S/Q, or cloud density, for a constant value $Q=1$, and ω_R taken from Table III. The chromaticity is zero. Pictures show (a) vertical and (b) horizontal side band spectra for the KEKB-LER, and (c) vertical spectra for the SPS.

beam force, the value of R_S/Q in the vertical plane can be a factor of 2 larger for $\omega_R\sigma_z/c>1$, whereas the Q value in both planes may be reduced by the nonuniform longitudinal beam distribution and by the beam size modulation due to the variation of the β function around the ring. The effect of changing R_S/Q is simply a shift along the horizontal axis of the figure. To estimate the effect of a reduced Q value, we repeat the mode-coupling calculation for $Q=1$, that is for a frequency spread $\Delta\omega\approx\omega_R/2$. This reduction in Q is introduced here *ad hoc*, in order to study the possible effect which the variation of beta functions around the ring and the nonuniform longitudinal charge density might have on the threshold. The result is depicted in Fig. 11. The threshold of mode coupling is only moderately affected by this change in Q. More precisely, now the instability threshold becomes

$$[cR_S/Q]_{\mathrm{thr},y}=1.9\times10^{7}\ \mathrm{m}^{-2},\quad \rho_{\mathrm{thr},y}\approx2.3\times10^{12}\ \mathrm{m}^{-3}, \tag{25}$$

$$[cR_S/Q]_{\mathrm{thr},x}=5.7\times10^{6}\ \mathrm{m}^{-2},\quad \rho_{\mathrm{thr},x}\approx2.0\times10^{12}\ \mathrm{m}^{-3}. \tag{26}$$

We note that $[cR_S/Q]_{\mathrm{thr},y}$ decreases, because $M_{0,-1}$ assumes a larger value for a lower Q at $\omega_c\sigma_z/c>1$. The vertical growth rate now increases to $\approx0.3\omega_s$ at $\rho_c=2\rho_{\mathrm{thr}}$, while the horizontal one does not change. As is emphasized before, R_S/Q in the vertical plane could increase by a factor of 2 for $\omega_R\sigma_z/c>1$ due to the effect of electron focusing under the influence of the beam force. To take this into account, we may consider a two times larger wake-field strength in the vertical plane, whereas the correction in the horizontal plane should be small (since $\omega_{e,x}\sigma_z/c=1.1$ and $\omega_{e,y}\sigma_z/c=2.8$). With this additional assumption, the estimate of the vertical threshold becomes $\rho_{\mathrm{thr}}\approx1\times10^{12}\ \mathrm{m}^{-3}$.

In the case of the SPS, reducing Q to 1, the threshold is

$$[cR_S/Q]_{\mathrm{thr},y}=1.8\times10^{6}\ \mathrm{m}^{-2},\quad \rho_{\mathrm{thr},y}\approx5.6\times10^{11}\ \mathrm{m}^{-3}, \tag{27}$$

$$[cR_S/Q]_{\mathrm{thr},x}=1.4\times10^{6}\ \mathrm{m}^{-2},\quad \rho_{\mathrm{thr},x}\approx5.4\times10^{11}\ \mathrm{m}^{-3}. \tag{28}$$

If here we also increase the wake-field amplitude by a factor of 2 to account for the electron focusing along the bunch, the threshold value decreases to $\approx2.7\times10^{11}\ \mathrm{m}^{-3}$.

We next discuss the instability using the fast blow-up method. The reasons for an alternative approach are the following. The mode-coupling calculation gives a reliable solution for instability rise times that are long compared with the synchrotron period. Also, in the mode-coupling calculation it is difficult to treat and interpret the case of nonzero chromaticity, since some modes are then already unstable at small current. If the instability growth time is small compared with the synchrotron period, it is not possible to compute the instability growth rate by expanding into synchrotron modes. In this case, we may estimate the associated instability threshold using the theory of vertical fast blow up first developed by Ruth and Wang [20] and later rederived by Kernel *et al.* [21]. A further advantage of this second approach is that, for conventional impedances, it is known to describe the dependence of the instability threshold on chromaticity in good agreement with observations [21].

The growth time is computed from the linearized Vlasov equation, taking into account the longitudinal particle dispersion due to energy spread and momentum compaction, but not the effect of the rf voltage. Without expanding into longitudinal modes, the threshold bunch population follows from the approximate solution of an integral equation [20,21]. Note that there are two minor differences between the formulas of [20] and [21]. First, the threshold estimates differ by a numerical factor of $\sqrt{3/2}$, and, second, one reference uses the effective impedance, the other the peak impedance. References [24,25] outline an alternative treatment of fast vertical instabilities. All these analytical treatments are based on the linearized Vlasov equation. Reference [20] determines an approximate solution to an eigenvalue equation.

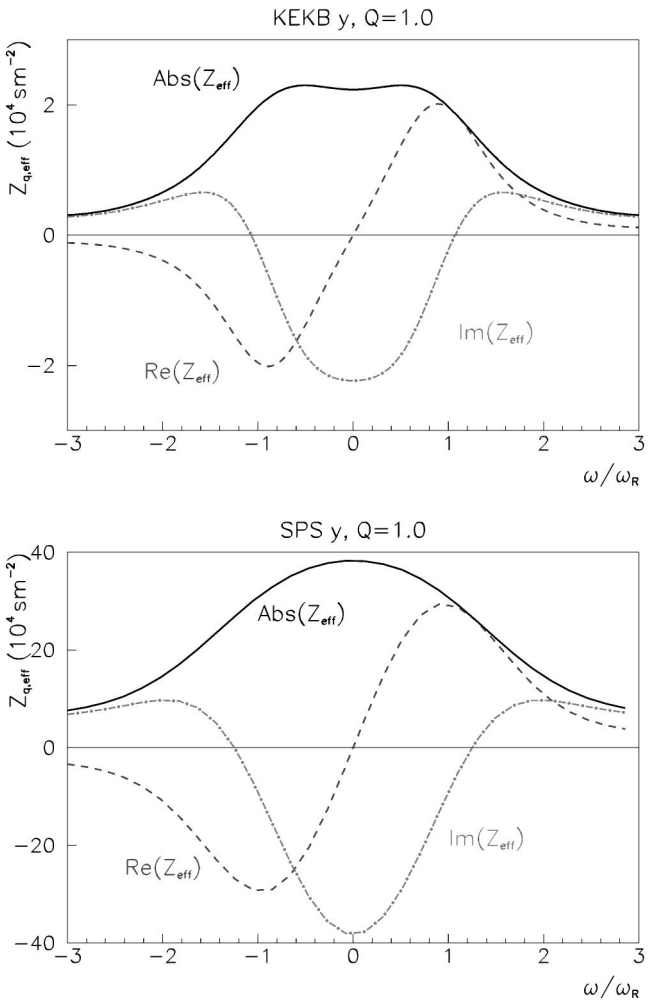

FIG. 12. Real, imaginary, and absolute values of the effective vertical impedance as a function of frequency in units of the resonant frequency for KEKB (upper) and SPS (lower). The impedance was computed using the parameters of Table III, but with $Q=1$ and two times enhanced wake amplitude.

The method proposed in Refs. [24,25] does not make this approximation, but involves complex mathematics and has been illustrated only for a simplified example wake field. We follow the approach of Refs. [20] and [21].

Applied to our resonator wake field, Eq. (19), the threshold of fast blow up [20,21] reads

$$N_{b,\mathrm{thr},x(y)} \approx \frac{4\pi L}{e^2 c^3 Z_0} \frac{4\eta(\Delta p/p)_{\mathrm{rms}} |\omega_R + \omega_{\xi,x(y)}| E\sigma_z}{\beta_{\perp,x(y)} |\mathrm{Re}[Z_{\mathrm{eff}}(\omega_{\max})]|}, \tag{29}$$

where E is the beam energy, Z_0 the vacuum impedance, η the slippage factor, $\beta_\perp$ the average transverse beta function, $\omega_{\max} \approx \omega_R$ the frequency at which the real part of the effective impedance, as defined in Ref. [21], is maximum, and $\omega_{\xi,x(y)} = Q'_{x(y)} c/(\eta L)$, the chromatic frequency shift. For a constant bunch current, Eq. (29) gives a threshold value for the effective impedance, or, equivalently, for the electron density (Fig. 12).

Inserting the parameter values of Table III, we compute the effective impedance as a function of frequency. Examples for KEKB and SPS are shown in Fig. 4. The effective impedances are $Z_{x,\mathrm{eff}} \approx 2.7\times 10^{-5}$ sm^{-2} and $Z_{y,\mathrm{eff}} \approx 7.7\times 10^{-5}$ sm^{-2} for the horizontal and vertical plane at KEKB and 1.9×10^{-5} sm^{-3} and 2.4×10^{-5} sm^{-3} for the horizontal and vertical plane at the SPS.

For the parameters of Table III, we then determine the threshold electron densities for the KEKB LER as

$$\rho_{\mathrm{thr},y} \approx [9.4\times 10^{11} + 2.4\times 10^{9} Q'_y] \ \mathrm{m}^{-3}, \tag{30}$$

$$\rho_{\mathrm{thr},x} \approx [1.1\times 10^{12} + 7.0\times 10^{9} Q'_x] \ \mathrm{m}^{-3}, \tag{31}$$

and for the CERN SPS as

$$\rho_{\mathrm{thr},y} \approx [2.0\times 10^{11} + 2.9\times 10^{11} \xi_y] \ \mathrm{m}^{-3}, \tag{32}$$

$$\rho_{\mathrm{thr},x} \approx [2.0\times 10^{11} + 3.6\times 10^{11} \xi_x] \ \mathrm{m}^{-3}, \tag{33}$$

where, in the second case, we have converted Q' into $\xi_{x(y)} = Q'_{x(y)}/Q_{\beta,x(y)}$, as used in the SPS control room. These thresholds coincide with the corresponding values from the TMCI calculation within a factor of 2. We observe again that for both SPS and KEKB the horizontal and vertical instabilities are about equally strong. For KEKB the dependence on the chromaticity is rather weak, whereas for the SPS an increase in chromaticity by $\Delta\xi_{x,y} \approx +0.6$ is predicted to double the instability threshold. This is roughly in agreement with observations.

If we repeat the same exercise as for the TMCI calculation, and again consider a reduced value $Q=1$ for all cases, the effective impedances become $Z_{y,\mathrm{eff}} \approx 3.4\times 10^{-5}$ sm^{-2} and $Z_{x,\mathrm{eff}} \approx 1.9\times 10^{-5}$ sm^{-2} for KEKB, and $Z_{y,\mathrm{eff}} \approx 5.8\times 10^{-3}$ sm^{-2} and $Z_{x,\mathrm{eff}} \approx 5.2\times 10^{-3}$ sm^{-2} for the SPS. In this case, the threshold electron densities for the KEKB LER are

$$\rho_{\mathrm{thr},y} \approx [2.2\times 10^{12} + 5.8\times 10^{9} Q'_y] \ \mathrm{m}^{-3}, \tag{34}$$

$$\rho_{\mathrm{thr},x} \approx [1.5\times 10^{12} + 9.7\times 10^{9} Q'_x] \ \mathrm{m}^{-3}, \tag{35}$$

and for the CERN SPS are

$$\rho_{\mathrm{thr},y} \approx [3.4\times 10^{11} + 4.6\times 10^{11} \xi_y] \ \mathrm{m}^{-3}, \tag{36}$$

$$\rho_{\mathrm{thr},x} \approx [3.0\times 10^{11} + 5.4\times 10^{11} \xi_x] \ \mathrm{m}^{-3}. \tag{37}$$

Thus, the threshold values obtained from the theory of fast blow up with $Q=1$ agree almost perfectly with those predicted by the TMCI calculation. We again want to emphasize that the wake-field amplitude may increase by a factor of 2 for $\omega_R \sigma_z/c > 1$, especially in the vertical plane of KEKB.

V. CONCLUSION

We have studied the wake field induced by the electron cloud using both analytical and simulation approaches. The wake field is approximated by a resonator, whose parameters (R_S/Q, ω_R, and Q) can be determined by either approach. Results are listed in Tables II and III. The analytic theory

gives the resonator parameters for a rigid Gaussian beam and an electron cloud of equal rms size, with results as shown in Eqs. (5), (6), (10), and (11). However, in this approach Q is infinite, because the wake field has a unique frequency and does not decay. On the other hand, the simulation includes the nonlinearity of the beam-cloud interaction as well as the effect of the cloud size. The strength of the simulated wake field (R_S/Q) increases for larger cloud sizes, while Q is reduced to a finite value due to the nonlinear force. For a flat beam $(\sigma_x/\sigma_y \sim 7)$, the strength of the vertical wake increases two times for increasing cloud size, while that of the horizontal wake increases much further. The strength of the horizontal wake $[cR_S/Q]_x$ is about $\sqrt{\sigma_y/\sigma_x} \times [c/R_S/Q]_y$. This factor indicates the number of electrons contributing to the wake force. For a round beam $(\sigma_x/\sigma_y \sim 1.7)$, the strength of the simulated wake force in both planes is 3–5 times larger than the analytic one. The empirical relation $[cR_S/Q]_x/[cR_S/Q]_y = \sqrt{\sigma_y/\sigma_x}$ is also fulfilled for the round beam. The resonator frequency ω_R slightly differs between the simulation and the analytical calculation. It is about 25% larger for the analytic estimate. The wake force was found to be linear for transverse perturbation amplitudes smaller than the rms beam size. This fact suggests that the instability saturates at an amplitude comparable to the beam size.

Electrons in the cloud are gathered near the beam due to the attractive beam force, with the result that the electron-cloud density inside the beam increases along a bunch. This density increase progresses on a time scale of $1/\omega_R$. As a result of this density increase, the simulated wake field is enlarged along the bunch. The simulated enlargements are a factor 2 for the vertical wake force of the KEKB-LER $(\omega_R \sigma_z/c = 2.8)$ and about 50% for the SPS $(\omega_R \sigma_z/c = 1.2)$. There is little enlargement for KEKB-LER in the horizontal plane $(\omega_R \sigma_z/c = 1.1)$.

Our wake-field computation did not take into account the nonuniform longitudinal charge distribution inside a bunch, or the beam size modulation around the ring due to the variation of beta function. Both effects will decrease the Q value.

The single bunch instability caused by the simulated wake field was analyzed by both mode-coupling theory and by the theory of fast blow up. In the former case, we considered only the lowest radial mode and calculated the spectra of betatron side bands $(|l| \leq 4)$ for various values of the electron-cloud density or cR_S/Q. The thresholds of the mode-coupling (strong head-tail) instability were obtained as $\rho_c \approx 1.7 \times 10^{12}$ m^{-3} in the vertical plane and $\rho_c \approx 3.3 \times 10^{12}$ m^{-3} in the horizontal plane for KEKB-LER, and $\rho_c \approx 3.8-4.4 \times 10^{11}$ m^{-3} for the CERN SPS, using the wake-field parameters of Table III. We next examined the effect of a reduction in the Q value to $Q=1$, thereby roughly approximating the effect of the resonance frequency spread along the bunch and around the ring. For the reduced Q value, we obtained the modified thresholds $\rho_c \approx 2.3 \times 10^{12}$ m^{-3} vertically and $\rho_c \approx 2.0 \times 10^{12}$ m^{-3} horizontally for KEKB-LER, and $\rho_c \approx 5.5 \times 10^{11}$ m^{-3} for the CERN SPS. The threshold values could be reduced by the wake-field enlargement due to the electron density increase along the bunch. The enlargement is especially conspicuous for the vertical wake force of KEKB-LER, as discussed above. The computed vertical threshold for KEKB-LER is roughly consistent with that of a tracking simulation, $\rho_c \approx 5 \sim 10 \times 10^{11}$ m^{-3} [5,22,23]. In tracking simulations, a horizontal instability has not yet been reported. More studies are needed for this case.

In addition to the mode-coupling calculation, we have computed threshold cloud densities for the fast blow-up (or ''post head-tail'') instability [20,21], using the approximate wake fields inferred from our simulation. The values so obtained roughly agree with those from the TMCI calculation. The theory of fast blow up also gives the dependence on the chromaticity. The instability threshold at the SPS is predicted to be more sensitive to the chromaticity than that at KEKB, which is consistent with observations.

Finally, all wake fields discussed in this paper were computed for a region free of external magnetic fields. The horizontal wake field will likely be suppressed inside a bending magnet. The vertical wake in a bending magnet should be similar to that calculated here. The effect of a weak solenoid field on the wake function is less clear. These questions will be the subject of future studies.

ACKNOWLEDGMENTS

This work was done in the summer of 2000 while one of the authors (K.O.) was visiting CERN. The authors thank F. Ruggiero for providing the opportunity for their collaboration, and they acknowledge helpful discussions with H. Fukuma, K. Oide, and G. Rumolo.

[1] K. Oide *et al.*, in *Proceedings of the International Workshop on Performance Improvement of Electron-Positron Collider Particle Factories, KEKB Proceedings 99-24, 2000*, edited by K. Akai *et al.* (KEK, Tsukuba, 2000), p. 12; H. Fukuma *et al.* (to be published).

[2] J. Seeman, in *Proceedings of the Seventh European Particle Accelerator Conference (EPAC 2000), Vienna, 2000*, edited by J.-L. Laclare *et al.* (Austrian Academy of Sciences Press, Vienna, 2000), p. 38.

[3] W. Höfle *et al.*, in *Proceedings of the Seventh European Particle Accelerator Conference (EPAC 2000), Vienna, 2000*, edited by J.-L. Laclare *et al.* (Austrian Academy of Sciences Press, Vienna, 2000), p. 259; G. Arduini *et al.*, *ibid.*, p. 939.

[4] F. Zimmermann, CERN-SL-Note-2000-004 AP, 2000 (unpublished).

[5] K. Ohmi and F. Zimmermann, Phys. Rev. Lett. **85**, 3821 (2000).

[6] T.O. Raubenheimer and F. Zimmermann, Phys. Rev. E **52**, 5487 (1995).

[7] K. Ohmi and F. Zimmermann, in *Proceedings of the Seventh European Particle Accelerator Conference (EPAC 2000), Vienna, Austria, 2000*, edited by J.-L. Laclare *et al.* (Austrian

Academy of Sciences Press, Vienna, 2000), p. 1164; KEK preprint 2000-53.
[8] K. Ohmi, Phys. Rev. Lett. **75**, 1526 (1995).
[9] D. Neuffer *et al.*, Part. Accel. **23**, 133 (1988); Nucl. Instrum. Methods Phys. Res. A **321**, 1 (1992).
[10] R. Macek (to be published).
[11] K.J. O'Brien, J. Appl. Phys. **65**, 9 (1989).
[12] G. Rumolo *et al.* CERN Report No. CERN-SL-2001-014-AP, 2001 (unpublished).
[13] For example, A. Chao, *Physics of Collective Instabilities in High Energy Accelerators* (Wiley, New York, 1993), and references therein.
[14] M. A. Furman and G. R. Lambertson, in *Proceedings of the 1997 Particle Accelerator Conference, Vancouver, 1997*, edited by M. Comyn *et al.* (IEEE, Piscataway, 1997), p. 1617.
[15] F. Zimmermann, H. Fukuma, and K. Ohmi, CERN Report No. CERN-SL-Note-2000-061, 2000 (unpublished).
[16] M. Furman and A. A. Zholents, in *Proceedings of the 1999 Particle Accelerator Conference, New York, 1999*, edited by A. Luccio and W. MacKay (IEEE, Piscataway, 1997), p. 1794.
[17] M. Bassetti and G. Erskine, CERN Report NO. CERN ISR TH/80-06, 1980.
[18] See p. 75 in Ref. [13].
[19] K. Yokoya, Y. Funakoshi, E. Kikutani, H. Koiso, and J. Urakawa, KEK Report No. 89-14, 1989 (unpublished).
[20] R.D. Ruth and J. Wang, IEEE Trans. Nucl. Sci 28 (1981).
[21] P. Kernel, R. Nagaoka, J.-L. Revol, and G. Besnier, in *Proceedings of the Seventh European Particle Accelerator Conference (EPAC 2000), Vienna, 2000*, edited by J.-L. Laclare *et al.* (Austrian Academy of Sciences Press, Vienna, 2000), p. 1133.
[22] G. Rumolo, F. Ruggiero, and F. Zimmermann, Phys. Rev. ST Accel. Beams **4**, 012801 (2001); G. Rumolo, F. Zimmermann, H. Fukuma, and K. Ohmi, CERN-SL-2001-040-AP, 2001.
[23] K. Ohmi, KEK Report No. 2001-33 (unpublished).
[24] D. Pestrikov, KEK Report No. 90-21, 1991, p. 18.
[25] N.S. Dikansky and D.V. Pestrikov, in *Physics of Intense Beams in Storage Rings* (Nauka, Moscow, 1989).